

times also determine effective electromagnetic operators; an  $E2$  effective-charge analysis for the  $A \approx 90$  nuclei similar to those for the Pb and Ca regions<sup>12</sup> is planned.

\*Work supported in part by the National Science Foundation.

†Present address: University of Tokyo, Tokyo, Japan.

‡Present address: Brooklyn College, City University of New York, New York, N. Y. 11234.

<sup>1</sup>N. Auerbach and I. Talmi, Nucl. Phys. **64**, 458 (1965); J. Vervier, Nucl. Phys. **75**, 17 (1966).

<sup>2</sup>J. B. Ball, J. M. McGrory, and J. S. Larsen, Phys. Lett. **41B**, 581 (1972).

<sup>3</sup>D. H. Gloeckner, M. H. Macfarlane, R. D. Lawson, and F. J. D. Serduke, Phys. Lett. **40B**, 597 (1972); D. H. Gloeckner and F. J. D. Serduke, Nucl. Phys. **A220**, 477 (1974), and private communication.

<sup>4</sup>B. A. Brown, P. M. S. Lesser, and D. B. Fossan, Bull. Amer. Phys. Soc. **18**, 1416 (1973).

<sup>5</sup>J. O. Newton, in *Nuclear Spectroscopy and Reactions*,

Part C, edited by J. Cerny (Academic, New York, 1974), pp. 185–227.

<sup>6</sup>H. Verheul and W. B. Ewbank, Nucl. Data Sheets **8**, 477 (1972).

<sup>7</sup>C. V. K. Baba, D. B. Fossan, T. Faestermann, F. Feilitzsch, M. R. Maier, P. Raghavan, R. S. Raghavan, and C. Signorini, J. Phys. Soc. Jpn., Suppl. **34**, 260 (1973).

<sup>8</sup>M. Grecescu, A. Nilsson, and L. Harms-Ringdahl, Nucl. Phys. **A212**, 429 (1973).

<sup>9</sup>S. Matsuki, S. Nakamura, M. Hyakutake, M. Matoba, Y. Yosida, and I. Kumabe, Nucl. Phys. **A201**, 608 (1973).

<sup>10</sup>A. Graue, L. H. Herland, K. J. Lervik, J. T. Nesse, and E. R. Cosman, Nucl. Phys. **A187**, 141 (1972); M. R. Maier, thesis, Technische Universität, München, 1972 (unpublished), and private communication.

<sup>11</sup>H. P. Blok, thesis, Vrije Universiteit, Amsterdam, 1972 (unpublished).

<sup>12</sup>G. Astner, I. Bergstrom, J. Blomqvist, B. Fant, and K. Wikstrom, Nucl. Phys. **A182**, 219 (1972); B. A. Brown, D. B. Fossan, J. M. McDonald, and K. A. Snover, Phys. Rev. C **9**, 1033 (1974).

## Experimental Measurement of the Form Factors of the Decay $K_L^0 \rightarrow \pi^\pm e^\mp \nu \bar{\nu}$

R. Blumenthal,\* S. Frankel, J. Nagy,† L. Resvanis, O. Van Dyck,§ and R. Werbeck§  
*Department of Physics, University of Pennsylvania, Philadelphia, Pennsylvania 19174*

and

R. Winston

*Department of Physics, University of Chicago, Chicago, Illinois 60637*

and

V. Highland

*Department of Physics, Temple University, Philadelphia, Pennsylvania 19122*

(Received 18 September 1974)

We have analyzed 25 000  $K_{e3}$  decays, reconstructed to the center of mass by measurement of the  $K_L^0$  momentum from time of flight and measurement of the  $\pi$  and  $e$  momenta with a spark-chamber-magnet spectrometer. Using the linear parametrization of the vector form factor  $f_+(q^2) = 1 + \lambda_+(q^2/m_\pi^2)$  we find  $\lambda_+ = 0.0270 \pm 0.0028$ . Upper limits for the scalar ( $f_s$ ) and tensor ( $f_t$ ) form factors at the 68% confidence level are  $f_s/f_+ < 0.04$ ,  $f_t/f_+ < 0.23$ , corresponding to intensity ratios  $I_s/I_v < 0.3\%$  and  $I_t/I_v < 0.4\%$ .

As part of an experimental study of  $K_L^0$  decays we have made a new measurement of the vector form factor  $f_+(q^2)$ , and set new limits on the scalar ( $f_s$ ) and tensor ( $f_t$ ) form factors in  $K_{e3}$  decay ( $K_L^0 \rightarrow \pi^\pm e^\mp \nu$ ). These data serve to resolve discrepancies in published results for the  $K_{e3}^0$  vector form factor and provide definitive data relating to the equality of  $K_{e3}^0$  and  $K_{e3}^+$  form factors.<sup>1</sup> This experiment utilized the rf structure of the proton beam of the Princeton-Pennsylvania

Accelerator to determine the momenta of the decaying  $K_L^0$  mesons, thus allowing for event reconstruction to the  $K_L^0$  center-of-mass system and kinematic suppression of possible  $K_{3\pi}$  contamination.

The vertical view of the apparatus (Fig. 1) is self-explanatory. Charged secondaries of the decays  $K \rightarrow \pi e \nu$ ,  $K \rightarrow \pi \mu \nu$ , and  $K \rightarrow \pi^+ \pi^- \pi^0$  inside the vacuum region were recorded in magnetostriptive spark chambers located before and after

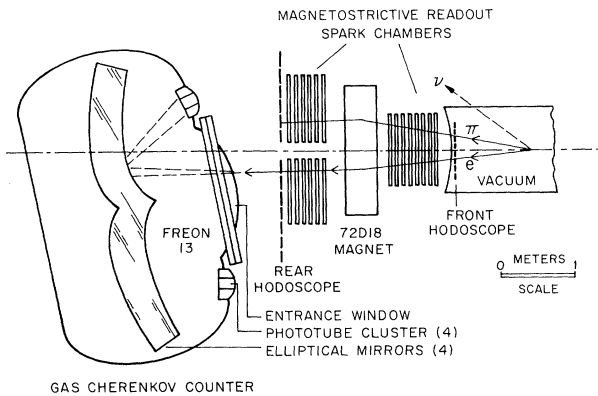


FIG. 1. Apparatus, top view.

an analyzing magnet. Events were recorded when any two of the front scintillation hodoscope counters and any two of the rear scintillation hodoscope counters fired. The signal heights and arrival times of the outputs of the phototube clusters in each of the quadrants of the pressurized gas Cherenkov counter,<sup>2</sup> and information on the arrival times of each of the charged secondaries at the hodoscope counters, were recorded on magnetic tape, along with the rf pulse time obtained from a timing counter<sup>3</sup> located near the internal accelerator target. Events for which (a) the track in the rear spark chambers coincided with the quadrant fired, (b) the Cherenkov and rear hodoscope signals were within 10 nsec, and (c) only one track entered the Cherenkov aperture were accepted as  $K_{e3}$  candidates. The Freon-filled Cherenkov counter was insensitive to pions and muons except for the small amount of scintillation light produced in Freon. Such triggers, not eliminated by the Cherenkov-hodoscope timing requirement, were eliminated by use of a pulse-height cut on the phototube cluster signals.

By measuring the  $K_L$  momentum and the momenta of the charged secondaries, and by assigning  $\pi$  and  $e$  masses to the secondaries, the square  $(MM)^2$  of the missing mass,  $(E_K - E_\pi - E_e)^2 - (\vec{P}_K - \vec{P}_\pi - \vec{P}_e)^2$ , of an event can be calculated. Figure 2 shows a comparison of the expected<sup>4</sup> and observed distribution in  $(MM)^2$  for events bending inward as they traverse the magnet ( $U$ 's) and those bending outward ( $Y$ 's). It is apparent that the  $(MM)^2$  resolution is much better for  $U$ 's than for  $Y$ 's. Also shown is the relative number of  $K_{3\pi}$  decays for each sample without the Cherenkov requirement. One possible source of background is a  $K_{3\pi}$  decay in which the  $\pi^0$ -decay  $\gamma$  rays trigger the Cherenkov counter. Unfortunate-

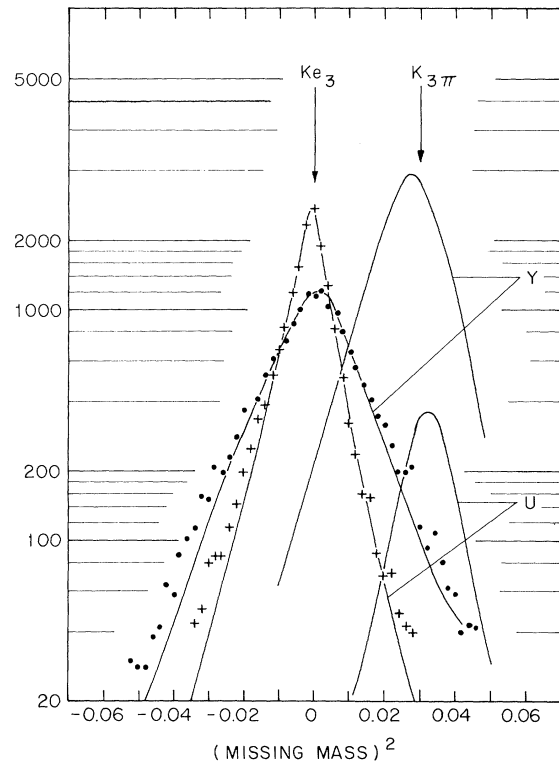


FIG. 2. The number of events, plotted on a logarithmic scale, versus missing mass for the data (+denotes  $U$ ,  $\circ$  denotes  $Y$ ), showing Monte Carlo results for  $K_{e3}$  and  $K_{3\pi}$ .

ly,  $K_{3\pi}$  events reconstructed as  $K_{e3}$  preferentially simulate high- $q^2$   $K_{e3}$  events. Thus, such background would be much more serious for  $Y$ 's than for  $U$ 's.

We have applied a  $(MM)^2$  cut of  $<0.015$   $(\text{GeV})^2$  to all our data. The most pessimistic estimates of  $K_{3\pi}$  contamination are  $<0.2\%$  for  $U$ 's and  $<0.7\%$  for  $Y$ 's.

For each event the square of the four-momentum transfer to the leptons,  $q^2 = (E_\nu + E_e)^2 - (\vec{P}_\nu + \vec{P}_e)^2$ , is computed. Figure 3 shows the relative efficiency of our apparatus, as a function of the momentum transfer  $q^2$ , for the  $U$  and  $Y$  configurations. For comparison,  $q^2$  efficiencies for two previous experiments [Bisi *et al.*,<sup>5</sup> labeled "CERN," and Chien *et al.*,<sup>6</sup> labeled "Hopkins-UCLA"] are shown. The  $Y$ 's show exceedingly rapid efficiency variations especially at high  $q^2$ . For all these reasons it is instructive to compare form factors for  $U$  and  $Y$  events separately.

Plots of  $f(q^2)$  for events with  $(MM)^2 < 0.015$   $(\text{GeV})^2$  which reconstruct to the center of mass are shown separately for  $U$ 's and  $Y$ 's in Fig. 4

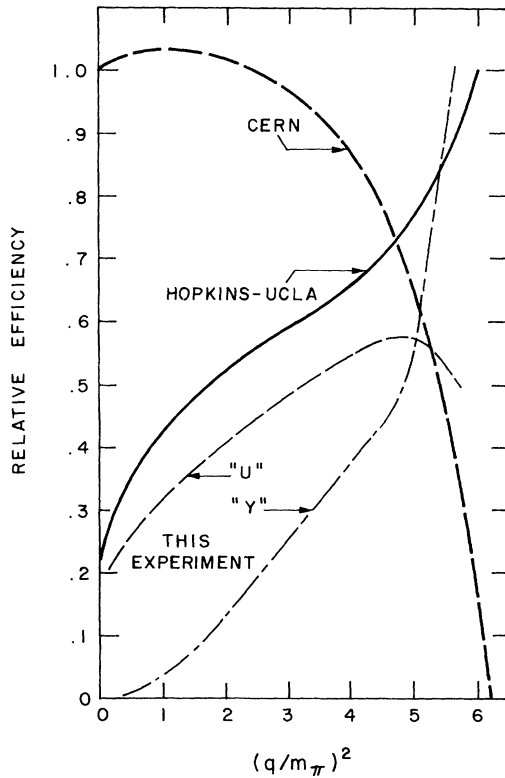


FIG. 3. Efficiency of detection of  $K_{e3}$  events versus square of momentum-transfer for two configurations ( $U$  and  $Y$ ) in our experiment and for two other dissimilar experiments.

normalized to an extensive Monte Carlo simulation. One striking feature of these plots is the pronounced turn-up in the highest  $q^2$  bin. Another feature is the good agreement between  $U$ 's and  $Y$ 's if the point at  $q^2 > 5.3$  is rejected. Table I shows the results of linear fits [ $f_+(q^2) = 1 + \lambda_+ q^2 / m_{\pi}^2$ ] to the data, with and without the highest  $q^2$  point, the goodness of fit for  $Y$ 's being considerably improved by rejection of the high- $q^2$  point. We have also found that quadratic fits to all points in the  $Y$  sample show poor  $\chi^2$  fits. As we have seen (Figs. 2 and 3), the  $Y$  sample in this region is most susceptible to  $K_{3\pi}$  contamination and efficiency variation. Finally we have found that the high- $q^2$  point, for both  $U$ 's and  $Y$ 's, has not been stable to internal data cuts. For these reasons we drop this high- $q^2$  point from further consideration and consider all data in the region  $q^2 < 5.3$ . Our quadratic fit,  $f(q^2) = 1 + \lambda_+' q^2 / m_{\pi}^2 + \lambda_+'' q^4 / m_{\pi}^4$ , shows no need for  $\lambda_+'' \neq 0$ .

In complicated experiments such as this, which rely heavily on Monte Carlo simulation of the experiment to extract meaningful data, there is

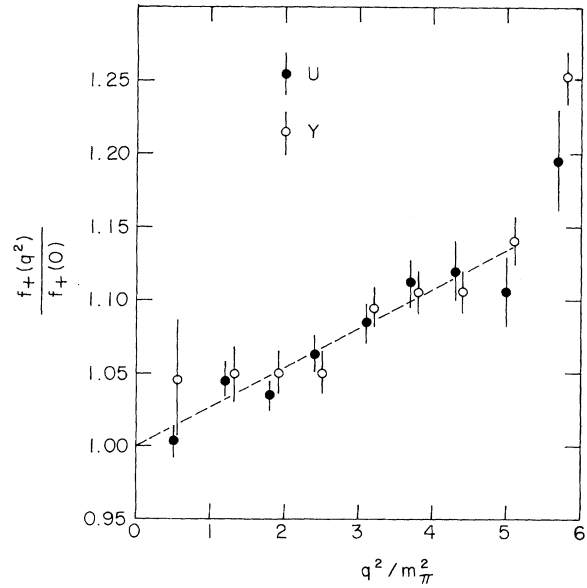


FIG. 4. Normalized  $f_+(q^2)$  data versus  $q^2/m_{\pi}^2$  for  $U$ 's and  $Y$ 's.

need to establish whether there are systematic nonstatistical errors either in simulation or event reconstruction. The method we employ is to examine the changes in  $\lambda_+$  in subsamples of two distinctly types: (a) those which have *very different*  $q^2$  efficiencies but are statistically independent, such as  $K$  momenta below 1000 MeV/c versus  $K$  momenta > 1000 MeV/c, downstream vertices versus upstream vertices, and  $U$ 's versus  $Y$ 's; and (b) those which have *identical*  $q^2$  efficiencies but are statistically independent, such as early acquired versus late acquired data, up-

TABLE I. Results of linear fits to the data.

Configuration	$\lambda_+$	$\chi^2/\text{degree of freedom}$
$U$ (all $q^2$ )	$0.0293 \pm 0.0036$	1.1
$Y$ (all $q^2$ )	$0.0379 \pm 0.0045$	3.5
All (all $q^2$ )	$0.0337 \pm 0.0026$	4.2
$U$ ( $q^2 < 5.3$ )	$0.0277 \pm 0.0038$	1.0
$Y$ ( $q^2 < 5.3$ )	$0.0243 \pm 0.0051$	0.7
All ( $q^2 < 5.3$ )	$0.0270 \pm 0.0028$	1.1
$K_L \rightarrow \pi^+ e^- \nu$	$0.0250 \pm 0.0041$	
$K_L \rightarrow \pi^- e^+ \nu$	$0.0297 \pm 0.0043$	
	$\lambda_+'$	
All ( $q^2 < 5.3$ )	$0.0319 \pm 0.0114$	1.1
	$\lambda_+''$	
	$0.0009 \pm 0.0020$	1.2

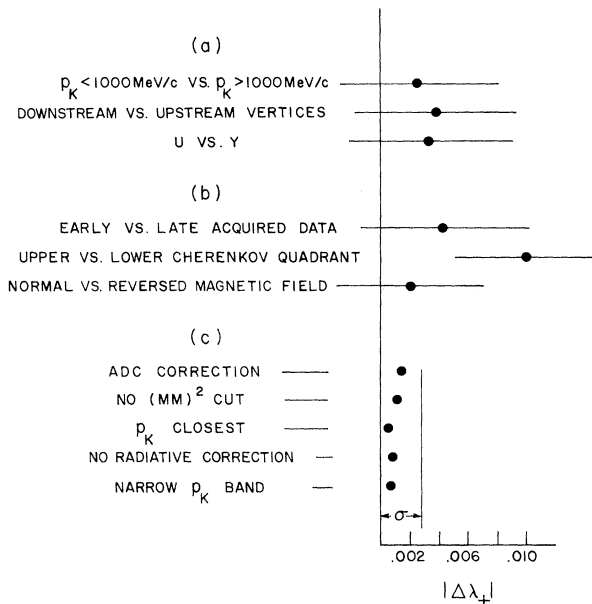


FIG. 5. Display of  $|\Delta\lambda_+|$  variations for subsets of data (a) with very different  $q^2$  efficiencies, (b) with identical efficiencies, and (c) for various corrections and cuts.

per versus lower Cherenkov counter quadrants, and normal versus reversed magnetic field data. Figure 5 shows our results for group A and group B subsamples and demonstrates that we have found no evidence for unexplained systematic errors. In the same figure we show [group (c)] the effect of various corrections or cuts to our value of  $\lambda_+$ : The "a.d.c. correction" shows the effect of accepting small pulses from the Cherenkov counter due to  $\pi$ - and  $\mu$ -induced scintillations and then correcting for the contamination of  $K_{\mu 3}$  and  $K_{3\pi}$ ; "no missing-mass cut" shows the effect of dropping our cut and correcting for the  $K_{3\pi}$  contamination thereby introduced. " $P_K$  closest" uses the  $P_K$  from our time-of-flight measurement to reconstruct events rather than using the lowest  $P_K$  solution. "Narrow  $P_K$  band" includes events with  $650 \text{ MeV}/c < P_K < 1350 \text{ MeV}/c$  rather than  $500 \text{ MeV}/c < P_K < 1500 \text{ MeV}/c$ ; the one-standard-deviation level of our final result is shown for comparison.

Finally, in Fig. 6 we present all our combined data, with fine binning, on a Marateck-Rosen plot.<sup>7</sup>  $\cos\beta$  is the angle between the electron and neutrino in the  $\pi$ - $\nu$  center of mass. In this plot  $q^2$ -independent vector and scalar form factors possess decay rates that are straight lines with slopes +1 and -1, respectively. In particular,

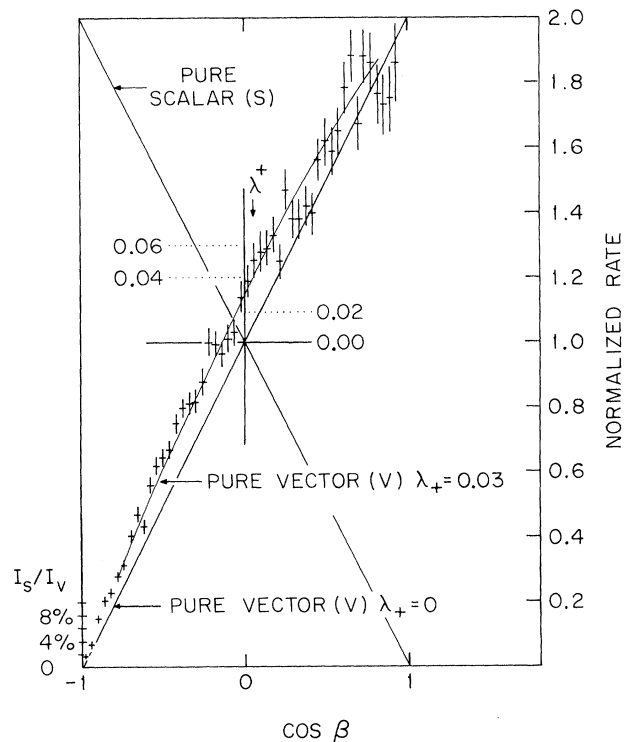


FIG. 6. Data displayed on a Marateck-Rosen plot. Values of  $\lambda_+$  and  $I_s/I_v$  can be read directly from the intercepts.

an upward bulge is produced by a  $\lambda_+ > 0$  vector form factor.  $\lambda_+$  can be read off directly from the scale at  $\cos\beta = 0$ . Similarly a nonzero intercept at  $\cos\beta = -1$  is evidence of scalar interaction and its magnitude can be read from the scale at  $\cos\beta = -1$ . From the analysis of the Marateck-Rosen plot we obtain  $I_s/I_v < 0.3\%$  or  $f_s/f_+ < 0.04$ . From a fit to the full Dalitz plot we obtain  $I_t/I_v < 0.4\%$  or  $f_t/f_+ < 0.23$  at a 68% confidence level.

Our result for  $\lambda_+$  is in good agreement with that of Bisi *et al.*<sup>5</sup> ( $0.023 \pm 0.005$ ) and Gjesdal *et al.*<sup>8</sup> ( $0.031 \pm 0.0025$ ), but is in poor agreement with that of Zdanis *et al.*<sup>9</sup> ( $0.044 \pm 0.006$ ).

For help with our  $K_L^0$  experiment we are indebted to many people: C. Banski, C. Clinesmith, M. Greenblatt, M. Hearn, J. Homer, G. Kouroupas, R. Marshall, M. Takats, W. Yang, C. West, and the Princeton-Pennsylvania Accelerator staff.

†Work supported in part by the U. S. Atomic Energy Commission.

\*Now at Bell Telephone Laboratory, Naperville, Ill. 60540.

‡Now at Johns Hopkins University, Baltimore, Md.

21218.

<sup>§</sup>Now at Clinton P. Anderson Meson Physics Facility, Los Alamos, N. M. 87544.

<sup>1</sup>Definitions of the form-factor formalism and the experimental status of  $K$ -meson form-factor measurements can be found in N. Barash-Schmidt *et al.*, Lawrence Berkeley Laboratory Report No. LBL-100, 1974 (unpublished), pp. xi, 51, 57.

<sup>2</sup>H. Hinterberger *et al.*, Rev. Sci. Instrum. **41**, 413 (1970).

<sup>3</sup>A water Cherenkov counter designed by D. Hutchinson.

<sup>4</sup>The time distribution of the proton bunch in the Princeton-Pennsylvania Accelerator was not known but is simulated by a Gaussian jitter introduced into the

Monte Carlo simulation. Many details of these experiments and the Monte Carlo calculation appear in J. Nagy, doctoral dissertation, University of Pennsylvania, 1974 (unpublished); and in R. Werbeck, doctoral dissertation, University of Pennsylvania, 1973 (unpublished).

<sup>5</sup>V. Bisi *et al.*, Phys. Lett. **36B**, 533 (1971).

<sup>6</sup>C.-Y. Chien *et al.*, Phys. Lett. **35B**, 261 (1971).

<sup>7</sup>S. Marateck and S. P. Rosen, Princeton-Pennsylvania Accelerator Report No. PPAR-8, 1969 (unpublished).

<sup>8</sup>S. Gjesdal *et al.*, as cited in V. Soergel, J. Phys. (Paris), Colloq. **34**, C1-83 (1973), p. 85.

<sup>9</sup>R. A. Zdanis *et al.*, as cited in V. Soergel, J. Phys. (Paris), Colloq. **34**, C1-83 (1973), p. 86.

## Spectrum of Heavy Mesons in $e^+e^-$ Annihilation\*

Barry J. Harrington, Soo Yong Park, and Asim Yildiz

*Lyman Laboratory of Physics, Harvard University, Cambridge, Massachusetts 02138*

(Received 11 December 1974)

The picture that charmed quarks are interacting with each other through a linear potential is used to analyze the particle spectrum in the high-energy annihilation process  $e^+e^- \rightarrow$  hadrons. With the newly found resonances at 3.1 and 3.7 GeV as input, we predict other resonances (in particular, one at approximately 4.0 GeV) and determine the hadronic width of the 3.1 and leptonic widths of the 3.1 and 3.7 resonances. Extending the linear potential to quarks without charm enables us to predict the charmed-particle threshold to be approximately 5 GeV.

Recent experiments concerning  $e^+e^- \rightarrow$  hadrons are providing a particularly instructive probe of hadronic structure and dynamics.<sup>1</sup> Especially interesting are the newly discovered narrow resonances at 3.1 and 3.7 GeV.<sup>2</sup> It has been argued<sup>3</sup> that the 3.1-GeV state is a  $^3S_1$  mesonic bound state of charmed<sup>4</sup> quarks, named "orthocharmonium."<sup>5</sup> We speculate that the 3.7-GeV state is a radial excitation of orthocharmonium and is only the first of a new spectrum of charmonium states.<sup>6</sup>

Explicitly, we study a quark system with exact gauge symmetry [e.g., color SU(3)] in which asymptotic freedom is realized in the short-distance limit, as in the scaling region of deep inelastic scattering.<sup>8</sup> In accordance with infrared slavery,<sup>9</sup> the gauge coupling grows with the quark separation, bring us into the domain described by a strong-coupling theory. Here, we use Schwinger<sup>10</sup> and Wilson<sup>11</sup> as guides and picture the quarks as confined by a flux of a gauge field, which leads to a linearly rising energy between the quarks.

These ideas are applied to  $e^+e^- \rightarrow$  hadrons by

considering the fate of the colored quark and antiquark produced from the single-photon remnant of the  $e^+e^-$  annihilation. Initially, the quark ( $q$ ) and antiquark ( $\bar{q}$ ) recede from each other almost freely, in accord with the ideas of asymptotic freedom. However, as the separation increases, a linear potential emerges and dominates. Now if the quarks do not fall into an energy eigenstate of the linear potential, they undergo a bremsstrahlung-type radiation with soft gauge photons (massless vector gluons). These gauge photons create a shower of quark pairs which form the final-state hadrons, as in the quark-parton explanation of scaling. But, if the quark energy coincides with an energy eigenvalue of the linear potential, then the quark is prohibited from producing the bremsstrahlung radiation and a bound state is formed. Since the  $q\bar{q}$  bound state is formed through a single-photon channel ( $J^{PC} = 1^{--}$ ), it must be a spin triplet, which we call orthocharmonium.<sup>5</sup> We assume that insofar as the quarks are in an energy eigenstate, their lifetime is sufficiently long so that their states are completely characterized by a linear poten-